Magnetic Moment of a Solid-State Plasma*

A. R. MOORE AND J. O. KESSLER
RCA Laboratories, Princeton, New Jersey
(Received 1 July 1963)

This report is concerned with the magnetic moment M of a plasma consisting of holes and electrons generated by light within a cylindrical semiconductor crystal immersed in a magnetic field. Macroscopic transport equations have been used to derive the dependence of M on field strength, mobility, and surface recombination conditions. In the limits of low and high surface recombination, the theoretical result demonstrates the transition between transverse equilibrium ($M=0$) and pure magnetic confinement ($M=-nkT/B$). Experiments using germanium and an inhomogeneous magnetic field directly measured the diamagnetic force exerted by the plasma on its scattering medium. An induction method utilizing a uniform magnetic field of strength up to 70 kG gave collateral results. The dependence of the moment on magnetic field strength, light intensity, temperature, and surface recombination velocity support the theory.

INTRODUCTION

THE magnetic moment of a dilute gas of electrically charged particles situated in a magnetic field depends on the dynamical state of the gas. In thermal equilibrium, all classical contributions to the magnetic moment vanish (Bohr-van Leeuwen theorem).[1] The remaining quantum contribution (Landau susceptibility) is small.[2] Under conditions of steady-state charged particle recombination and generation, a classical moment exists if there is transport in a direction perpendicular to the applied magnetic field.

The calculation and observation of the magnetic moment is much facilitated by a thorough knowledge of the properties of the gas—such as temperature, scattering processes, particle masses, and particle densities, together with their time rates of change. For this reason, germanium provides an ideal medium for such a study. The Landau susceptibility of equilibrium charge carriers has already been studied,[3] with the result of confirming the general theory and providing measurements of the anisotropic effective masses. The purpose of the present paper is to derive expressions for the expected steady state classical magnetic moment of a hole-electron plasma injected by light into a semiconductor and to compare these theoretical results with two independent sets of experimental measurements. One of the experiments performed directly measures the time variation of the magnetic moment resulting from the time variation of hole-electron density. The other experiment continues previous work[4,5] on the measurement of the force on the plasma-containing body due to the interaction of the magnetic moment with an inhomogeneous magnetic field.

The chief advantage of using a semiconductor rather than a gas plasma for these studies are the well-controlled conditions applying to both theory and experiment. Magnetic moment measurements in gases have been performed under varying conditions[6–8]; however, no direct force measurements are generally possible due to the nature of the system.[9] The theory of these effects has been discussed on several occasions. The work of Tonks,[10] Alfven,[11] and Lehnert[12] is representative. Transport of semiconductor plasmas in the presence of magnetic field has also been discussed. This work is summarized by Smith.[13] A mechanical effect due to the interaction of magnetic moment and field has also been reported.[14]

Although these treatments are closely related to the present work, they do not exactly match it, either in point of view, or in the detailed boundary conditions, which serve to demonstrate the variation of the classical magnetic moment between steady-state and equilibrium conditions.

THEORY

In the first part of this section, we derive the magnetic moment of a plasma in a scattering medium under

* Supported in part by the U. S. Office of Naval Research, contract No. NONR-3467(00).

[1] J. H. Van Vleck, *The Theory of Electric and Magnetic Susceptibilities* (Oxford University Press, New York, 1932), Chap. IV.

[2] See Ref. 1, Chap. XII.

[3] G. Busch and N. Helfer, Helv. Phys. Acta **201**, 27 (1954); G. Busch and E. Mooser, *ibid.* **26**, 611 (1953); C. Enz, *ibid.* **28**, 158 (1955); J. H. Crawford, H. C. Schweinler, and D. K. Stevens, Phys. Rev. **99**, 1330 (1955); A. Van Itterbeck, L. DeGreve, and W. Duchateau, Appl. Sci. Research Sect. B: **4**, 300 (1955); F. T. Hedgecock, Can. J. Phys. **34**, 43 (1956); R. Bowers, Phys. Rev. **108**, 683 (1957).

[4] J. O. Kessler and A. R. Moore, Phys. Rev. Letters **2**, 247 (1959).

[5] A. R. Moore and J. O. Kessler, Phys. Rev. Letters **4**, 121 (1960).

[6] M. Steenbeck, Wiss. Veroeffentl. Siemens **15**, 2, 1 (1936).

[7] T. C. Marshall and L. Goldstein, Phys. Rev. **122**, 367 (1961).

[8] W. M. Hooke, M. A. Rothman, and J. Adams, Bull. Am. Phys. Soc. **118**, 174 (1963).

[9] An exception is the measurement of the expansion force in a current-carrying toroidal gas plasma, S. Yoshikawa, R. M. Sinclair, J. O. Kessler, and W. L. Harries, Phys. Fluids **6**, 932 (1963).

[10] L. Tonks, Phys. Rev. **56**, 360 (1939).

[11] H. Alfvén, *Cosmical Electrodynamics* (Oxford University Press, New York, 1950), Chap. III.

[12] B. Lehnert, in *Proceedings of the Second United Nations International Conference on the Peaceful Uses of Atomic Energy, Geneva, 1958* (United Nations, Geneva, 1958), Vol. 32, p. 349.

[13] R. A. Smith, *Semiconductors* (Cambridge University Press, New York, 1961), Chap. V, VII, and VIII. Reference 14 also contains many useful references.

[14] O. Garreta and J. Grosvalet, in *Progress in Semiconductors*, edited by A. F. Gibson, P. Aigrain, and R. E. Burgess (John Wiley & Sons, New York, 1956), p. 165. See also A. Amith, Phys, Rev. **116**, 330 (1959).

arbitrary conditions of recombination and generation of the charge carriers. In the second part, we continue with a complete expression for the magnetic moment, using the particular generation-recombination conditions appropriate to the semiconductor plasma. Several simplifying assumptions are made:

(1) Steady-state conditions hold, i.e., $d\mathbf{v}/dt=(\partial/\partial t+\mathbf{v}\cdot\nabla)\mathbf{v}=0$, where $\mathbf{v}$ is the macroscopic drift velocity of charge carriers. The condition $(\mathbf{v}\cdot\nabla)\mathbf{v}\approx 0$ is equivalent to the condition $(\tau_i/\tau)\approx 0$, where τ is the particle recombination, and τ_i the scattering time.

(2) The magnetic field due to plasma currents is much smaller than the applied magnetic field $(8\pi nkT/B^2\ll 1)$.

(3) The standard ambipolar diffusion conditions apply.

(4) An isotropic, velocity-independent mobility, $\mu_i=e_i\tau_i/m_i$, where e_i is the charge and m_i is the mass of a particular class (i) of carriers, is used.

(5) The temperature of the plasma is the same as the temperature of the scattering lattice.

(6) The temperature is uniform.

(7) Carrier-carrier scattering is negligible.

Assumptions (1) and (2) arise from the experimental conditions to be described by the present theory. Assumption (4) is the most questionable, since there exist anisotropies in the effective masses and velocity dependence of the mean scattering time. Nevertheless, it has proved adequate for the description of similar effects in InSb.[15] It will be seen that it is also adequate for the present case, at least for $|\mu_i|B=|\omega_i|\tau_i\lesssim 10$, where $|\omega_i|$ is the cyclotron frequency of a particular charge carrier. Assumption (5) follows from the fact that the time scale of the experiment is $\sim 10^{10}$ times the relaxation time. The high thermal conductivity of germanium implies (6). Since the Coulomb scattering cross section is much less than the lattice scattering cross section in the temperature range studied, (7) is also very nearly valid.

The macroscopic drift velocity $\mathbf{v}_i$ of the ith class of carriers is given by[16]

$$n_i m_i(\partial/\partial t+\mathbf{v}_i\cdot\nabla)\mathbf{v}_i=n_i\mathbf{F}_i-\nabla p_i+\mathbf{P}_i, \tag{1}$$

where

$$\mathbf{F}_i=e_i(\mathbf{E}+\mathbf{v}\times\mathbf{B}), \quad \mathbf{P}_i=-(n_i m_i/\tau_i)\mathbf{v}_i\equiv -n_i(e_i/\mu_i)\mathbf{v}_i,$$

n_i is the particle density, m_i is the mass, τ_i is the mean scattering time, e_i is the charge, μ_i is the mobility, and $p_i=n_i kT$, the pressure. The subscript i refers to holes $(i=p)$ or electrons $(i=n)$, and μ_i is taken as a signed quantity. $\mathbf{E}$ and $\mathbf{B}$ are the electric and magnetic fields. Under steady-state conditions,

$$\mathbf{v}_i-(\mathbf{v}_i\times\mathbf{B})\mu_i=\mu_i\mathbf{E}-D_i(\nabla n_i/n_i)\equiv\mathbf{G}_i. \tag{2}$$

Here $D_i=(kT/e_i)\mu_i=(kT/e)|\mu_i|$ holds under the conditions of assumption (3). If $(\hat{e}_1,\hat{e}_2,\hat{e}_3)$ are a set of orthogonal right-handed unit vectors, and if $\mathbf{B}=B\hat{e}_3$, the solution of Eq. (2) is

$$(\mathbf{v}_i)=\frac{1}{1+\mu_i^2B^2}\begin{bmatrix}1 & \mu_iB & 0\\ -\mu_iB & 1 & 0\\ 0 & 0 & 1+\mu_i^2B^2\end{bmatrix}(\mathbf{G}_i). \tag{3}$$

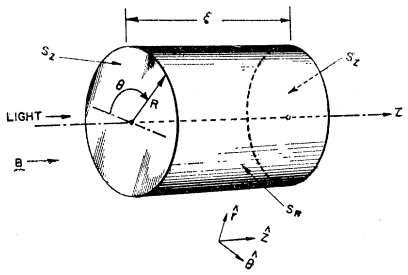

FIG. 1. Orientation of the cylindrical coordinate system with respect to the illuminated sample.

We choose cylindrical coordinates with unit vectors $(\hat{r},\hat{\theta},\hat{z})$ as illustrated in Fig. 1. It is assumed that $\nabla B=0$ and that the problem is symmetrical around the z axis. Then, since $E_r\neq E_r(\theta)$ and $\nabla\times\mathbf{E}=0$ imply $E_\theta=\text{const}\times r^{-1}$, and since we require $\mathbf{E}$ finite at the origin, we may set $G_{i,\theta}=0$. Then

$$\begin{aligned} v_{i,r}&=G_{i,r}(1+\mu_i^2B^2)^{-1}=-v_{i,\theta}/\mu_iB,\\ v_{i,z}&=G_{i,z}. \end{aligned} \tag{4}$$

The velocities v_r and v_θ give rise to the magnetic moment. To calculate them, assume that there is no radial charge accumulation. Then

$$j_{p,r}+j_{n,r}\equiv e(Pv_{p,r}-Nv_{n,r})=0, \tag{5}$$

where

$j_r=$ current density,

$P=P_0+p=$ total positive-charged particle density,

$N=N_0+n=$ total negative-charged particle density,

P_0 and $N_0=$ equilibrium particle densities, and

p and $n=$ particle densities injected by the incident light.

The ambipolar electric field required to satisfy Eqs. (4) and (5) is

$$E_r=\left[\frac{D_p/\phi_p-D_n/\phi_n}{P\mu_p/\phi_p-N\mu_n/\phi_n}\right]\cdot\frac{\partial n}{\partial r},$$

where $\phi_i=1+\mu_i^2B^2$. We have assumed $\nabla N=\nabla P=\nabla n=\hat{r}\partial n/\partial r$ and $n=p$. Inserting E_r into G_r and using Eqs. (3) and (4) we obtain

$$j_{p,r}\equiv -j_{n,r}=-eD_a(P,N,B)\partial n/\partial r. \tag{6}$$

Then

$$j_\theta\equiv j_{p,\theta}+j_{n,\theta}=(\mu_p+|\mu_n|)BeD_a(P,N,B)\partial n/\partial r, \tag{7}$$

[15] S. W. Kurnick and R. N. Zitter, J. Appl. Phys. **27**, 278 (1956).

[16] J. L. Delcroix, *Introduction to the Theory of Ionized Gases* (Interscience Publishers, Inc., New York, 1960), Chap. VIII.

where the ambipolar diffusion coefficient is given by

$$D_a(P,N,B)=D_pD_e(P+N)/(PD_p\phi_n+ND_n\phi_p). \quad (8)$$

When $n\gg N_0$, P_0,

$$D_a(P,N,B)=\frac{2D_pD_e}{D_p+D_e}\frac{1}{1+\mu^2B^2}\cdot\left\{1+\frac{N_0-P_0}{2n}\frac{D_p-D_n}{D_p+D_n}\times\left(\frac{1-\mu^2B^2}{1+\mu^2B^2}\right)[1-\cdots]\right\}, \quad (9)$$

where we have used $\mu^2\equiv\mu_p|\mu_n|$. If $N_0\gg n\approx P_0$,

$$D_a(P,N,B)=\frac{D_p}{1+\mu_p{}^2B^2}\left\{1+\frac{P_0+n}{N_0}\times\left[1-\frac{D_p}{D_n}\left(\frac{1+\mu_n{}^2B^2}{1+\mu_p{}^2B^2}\right)+\cdots\right]\right\}. \quad (10)$$

Use of the leading term of $D_a(N,P,B)$ in Eq. (9) is adequate under most of the conditions encountered in the present experiment. This term, which is the conventional ambipolar diffusion coefficient is written

$$D_a(B)=\frac{2D_pD_e}{D_p+D_e}\frac{1}{1+\mu_p|\mu_n|B^2}\equiv\frac{D}{1+\mu^2B^2}. \quad (11)$$

The magnetic moment per unit volume v due to the current density is[17]

$$\mathbf{M}=\frac{1}{2v}\int_v dv\,(\mathbf{r}\times\mathbf{j}). \quad (12)$$

For the geometry illustrated in Fig. 1, and for $\mathbf{j}=j_\theta\hat{\theta}$,

$$\mathbf{M}=\frac{\hat{z}}{R^2\zeta}[e(\mu_p+|\mu_n|)B]\times\int_0^\zeta dz\int_0^R r^2\frac{\partial n}{\partial r}D_a(P,N,B)dr, \quad (13)$$

$$\mathbf{M}=\hat{z}[e(\mu_p+|\mu_n|)B]\langle n(R)-2\bar{n}\rangle_z D_a(B), \quad D_a\neq D(z,r). \quad (13a)$$

In general n, and, therefore, $\partial n/\partial r$ and $D(P,N,B)$ are complicated functions of r and z. The nature of M is readily understood with the aid of the simplifying assumptions: $D_a(P,N,B)\approx D_a(B)$, $\zeta\to\infty$, and $\partial n/\partial r\approx-n\delta(r-R)$ (corresponding to the case of outward diffusion near the edge only), where $\int_0^R\to\int_0^\infty$, and δ is the Dirac delta function. Then

$$M=-en(\mu_p+|\mu_n|)\frac{B}{1+\mu^2B^2}\frac{2D_pD_n}{D_p+D_n}, \quad (14)$$

which becomes, with the aid of the Einstein relation,

$$M=-\frac{2nkT}{B}\frac{\mu^2B^2}{1+\mu^2B^2}. \quad (15)$$

This well-known equation leads to the result $M=-n'kT/B$ for $\mu_i{}^2B^2\equiv\omega_i{}^2\tau_i{}^2\to\infty$ (n' is the total charged-particle density). If $\partial n/\partial r=+n\delta(r-R)$, corresponding to inward radial diffusion of the plasma, and implying that j_θ is a paramagnetic current, $+|M|$, is obtained. This paramagnetic moment has been observed.[4] It illustrates the fact that "diamagnetism" is not an intrinsic property of the plasma. The sign of the macroscopically observable moment depends solely on the direction of transport. Only the individual particle orbits are intrinsically diamagnetic.

To evaluate the integral in Eq. (13) it is necessary to find $n(r)$. For simplicity, this problem is here treated in the approximation $\zeta\to\infty$, i.e., for planar flow perpendicular to B. The accurate treatment, important for small cylinder height ζ is given in Appendix II. The present calculation assumes uniform volume generation (g pairs/cm^3/sec created), uniform volume recombination (τ sec), and azimuthally independent surface recombination current $j_s=nS$ pairs/cm^2/sec, where S is a property of the semiconductor[18] and n is the density of pairs at the surface. Since pairs are actually created by light incident on the front surface of the cylinder (see Fig. 1), g will be represented in terms of S, D, τ, and I, where I is the number of pairs generated/cm^2/sec at the front surface (the light absorption takes place in a distance short compared to $L=\tau D$), and D is the usual, magnetic-field-independent, longitudinal ambipolar diffusion coefficient. The transverse diffusion coefficient is taken as $D_a(B)$. Since j_θ is not a function of θ and $j_{p,r}=-j_{n,r}$, and also suppressing the z dependence,

$$\frac{1}{r}\frac{\partial}{\partial r}(rj_{p,r})=e\left(g-\frac{n}{\tau}\right). \quad (16)$$

Using Eq. (6), and $D_a(B)\approx D_a(P,N,B)$,

$$\frac{1}{r}\frac{\partial}{\partial r}\left(D_a(B)\frac{\partial n}{\partial r}\right)=\frac{n}{\tau}-g, \quad (17)$$

$$\frac{1}{r}\frac{\partial}{\partial r}\left(r\frac{\partial n}{\partial r}\right)-\frac{n}{\Lambda^2}=-\frac{g}{D_a(B)}, \quad (18)$$

where $\Lambda^2=(1+\mu^2B^2)^{-1}L^2=D_a(B)\tau$. The boundary conditions are: $n(0)$ is finite and $-D_a(B)[\partial/\partial r(\ln n)]_{r=R}=S_R$, where S_R is the radial surface recombination velocity.

The solution is

$$n(r)=g\tau\left\{1-\frac{[S_R\Lambda/D_a(B)]I_0(r/\Lambda)}{I_1(R/\Lambda)+[S_R\Lambda/D_a(B)]I_0(R/\Lambda)}\right\}, \quad (19)$$

[17] L. Landau and E. Lifshitz, *Electrodynamics of Continuous Media* (Addison-Wesley Publishing Company, Inc., Reading, Massachusetts, 1960), p. 123.

[18] See Ref. 13, p. 297.

where I_ν is the νth-order Bessel function of imaginary argument. To obtain g in terms of I, we write the longitudinal equation for particle conservation, for both surface and volume generation. For volume generation,

$$\frac{\partial^2 n}{\partial z^2}-\frac{n}{L^2}=-\frac{g}{D}, \tag{20}$$

with boundary conditions: $n(z)\rightarrow 0$ as $z/L\rightarrow\infty$, and $-D[\partial/\partial z(\ln n)]_{z=0}=-S_z$. The solution is

$$n_g(z)=g\tau\left[1+\frac{(S_zL/D)e^{-z/L}}{1+(S_zL/D)}\right]. \tag{21}$$

Equation (20) also holds for surface generation if we set $g=0$. For that case the boundary conditions are: $n(z)\rightarrow 0$ as $z/L\rightarrow\infty$ and $-D[\partial/\partial z(\ln n)]_{z=0}=I-nS_z]_{z=0}$, where S_z is the front surface recombination velocity. The solution is

$$n_I(z)=\frac{IL}{D}\frac{e^{-z/L}}{1+(S_zL/D)}. \tag{22}$$

Since the average density must be equal, we set $\int_0^\zeta[n_g(z)-n_I(z)]dz=0$, giving

$$g\tau\cong\frac{I\tau}{\zeta}\frac{1}{1+(S_zL/D)}. \tag{23}$$

Combining Eqs. (23) and (19), we may evaluate Eq. (13) for the magnetic moment.

$$M=-e(\mu_p+|\mu_n|)B\left[\frac{D_a(B)I_2(R/\Lambda)[S_R\Lambda/D_a(B)]}{I_1(R/\Lambda)+[S_R\Lambda/D_a(B)]I_0(R/\Lambda)}\right]\times\left[\frac{I\tau}{\zeta}\frac{1}{1+(S_zL/D)}\right]. \tag{24}$$

When $R\gg\Lambda$, we may approximate

$$I_\nu(R/\Lambda)\approx e^{R/\Lambda}(2\pi R/\Lambda)^{-1/2}.$$

In the present experiment $R/\Lambda\geqq 5$. Also writing $D_a(B)$ and Λ in terms of D, L, and B, and using the Einstein relation, we obtain

$$M\approx-\frac{kT\mu^2B}{(1+\mu^2B^2)^{1/2}}\cdot\frac{(S_RL/D)}{1+(S_RL/D)(1+\mu^2B^2)^{1/2}}\times\left[\frac{2I\tau}{\zeta}\frac{1}{1+(S_zL/D)}\right]. \tag{25}$$

The last term plays the role of total particle density, $2n$. Since Eq. (25) assumes $R\gg\Lambda$, it may be expected to hold as well for square cross-section samples of similar dimensions.

For $(S_RL/D)\rightarrow\infty$, or $\mu^2B^2\equiv\mu_p|\mu_n|B^2\rightarrow\infty$, Eq. (25) becomes identical with Eq. (15), corresponding, respectively, to the equivalent cases of perfectly absorbing boundary, or magnetic confinement (apart from the "pressure" exerted by lattice collisions). If $S_R\rightarrow 0$, $M\rightarrow 0$, corresponding to the Bohr-van Leeuwen theorem case of transverse equilibrium, or perfectly reflecting walls. The present semiconductor case, with finite and variable S_RL/D is, therefore, one in which the transition between these classical limiting cases may be observed.

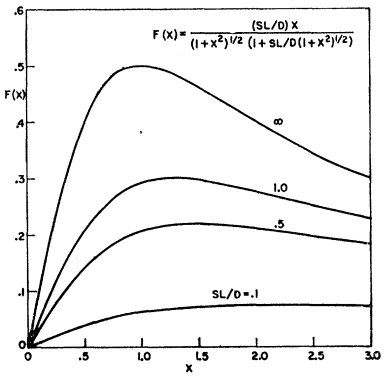

FIG. 2. Functional form of the magnetic moment as a function of SL/D. Here we consider only the surface recombination velocity S of the cylindrical surface (S_R). The variable $x=(\mu_e\mu_p)^{1/2}B=(\omega_e\tau_e\omega_p\tau_p)^{1/2}B$. Equation (25).

The variation of the M as a function of $\mu B=(\omega_p\tau_p\omega_n\tau_n)^{1/2}$ is shown in Fig. 2. It is seen that the general shape is not a strong function of S_RL/D; for $\infty>S_RL/D\geq\frac{1}{4}$ the location of the maximum of M varies between $1\geq(\mu B)_{\max}\geq 1.7$.

EXPERIMENTAL WORK

A. General

The magnetic moment [Eq. (13)] derived above arises from the nonequilibrium component of the plasma. In our experiments this component, consisting of holes and electrons, was generated by illuminating the specimen with light. Since the magnetic properties measured in the experiment are a direct function of the intensity and time variation of the incident light, as well as of the magnetic field and specimen properties, we refer to the observed effects as "photomagnetism."

The photomagnetism effects in germanium have been studied by two different methods. The experiments at low magnetic field ($B<11$ kG) were done with an apparatus,[19] shown schematically in Fig. 3 which measures the force on the magnetic moment in an inhomogeneous magnetic field. The apparatus basically uses the Faraday method; however, only the alternating component of the force is measured when the sample is illuminated by light modulated at the detection frequency. The result is that only the change in magnetic

[19] J. O. Kessler and A. R. Moore, Rev. Sci. Inst. 33, 478 (1962).

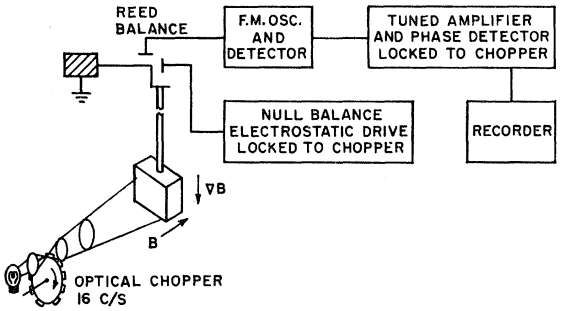

FIG. 3. Experimental arrangement used at low fields ($B<11$ kG). It measures the force on the magnetic moment generated by the light, in an inhomogeneous field.

susceptibility χ for a given change in light intensity is obtained. Slow drifts in the total χ, due, for instance, to specimen temperature changes, are ignored. By this means a detection limit of about 10^{-11} cgs units was achieved. Thus, the observed signal, which usually corresponded to a $\Delta\chi$ of about 10^{-9} cgs units, could be measured to a few percent. Systematic errors due to uncertainties in the knowledge of the magnitude of the magnetic field and the calibration of the apparatus, as well as variations in light input were of similar magnitude.

The force is given by

$$F_y(t)=M_z(t)\partial B_z/\partial y=\chi(t)B_z\partial B_z/\partial y, \qquad (26)$$

where y is in the vertical direction, z the horizontal (along $\mathbf{B}/B$). The field gradient, of magnitude $(\partial B_z/\partial y)/B_z\approx -0.1$ cm^{-1}, was obtained by specially shaped pole pieces.[20]

Whenever results are plotted versus magnetic field, it is the average field that is referred to. Since the samples were 1 cm in length along the gradient, the actual field varied $\pm 5\%$ from the mean. Over-all specimen dimensions were usually $x=y=10$ mm, $z=5$ mm, where x is taken perpendicular to y and z.

At high magnetic fields (11 kG$<B<$70 kG), an induction method was used to measure the derivative of magnetic moment with respect to the light intensity. This experiment made use of a uniform magnetic field generated by discharging a condenser bank into a solenoid. The departure from uniformity did not exceed 2% over the specimen volume. In this method, a germanium crystal located inside the solenoid is illuminated with a single short pulse of light at some time during the magnetic field discharge. The change in magnetic moment due to the light is detected by a set of pick-up coils surrounding the sample. In many respects the experiment is similar to the impulse method of measuring the de Haas–van Alphen effect in metals.[21]

[20] D. R. Fredkin collaborated in the design.

[21] D. Schoenberg, in *Progress in Low Temperature Physics* (North-Holland Publishing Company, Amsterdam, 1957), Vol. 2, 226.

The experimental arrangement is shown in Fig. 4 together with a block diagram of the electronic circuitry. Further details concerning this method are discussed in Appendix I.

In both the force measurements at low field and the direct magnetic-moment measurements at high field, the light beam generating the hole electron plasma was directed parallel to the magnetic field. All but the front faces of the specimens were coated with an opaque nitrocellulose paint in order to prevent illumination of the sample edges which would lead to inward carrier concentration gradients, transverse to **B**, which would give rise to a paramagnetic moment. The surface was otherwise unaffected by the paint.

B. Specimen Properties

The experiments reported in this paper were done with high resistivity ($\rho>20$ Ω-cm) germanium single-crystal specimens. At room temperature, the equilibrium carrier density in such material is $10^{14}\geq P_0, N_0$ cm^{-3}.

Since the time varying photomagnetic moment $M(t)$ depends on the spatial and temporal variation of the carrier density, it was necessary to know the relevant parameters describing recombination, photogeneration, and transport of carriers.

The total photopair density was measured as a function of light intensity and temperature. The photopair density Δn versus light intensity I at room temperature was obtained by measurement of the conductance change in a suitably shaped specimen. As shown in Fig. 5, the photoconductivity is linear up to $\Delta n\approx 10^{14}$/cm^3 and, thereafter, is proportional to approximately the $\frac{1}{2}$ power of light intensity I. Since, in general, in the steady state $\Delta n=g\tau$, where g is the generation rate proportional to light intensity I and τ is the lifetime, this implies that $\tau\propto 1/\Delta n$ in the illumination range in which $\Delta n\propto I^{1/2}$. This behavior is common and expected in high-resistivity germanium when $\Delta n>n_0$.[22] For our purposes, the important point is that the room temperature photomagnetism experiments were done in such an illumina-

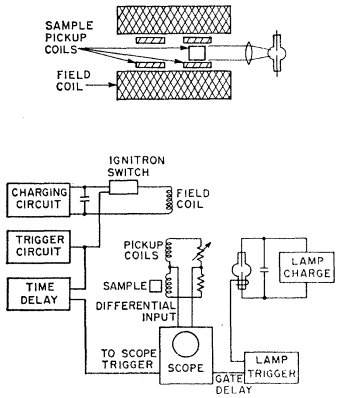

FIG. 4. Experimental arrangement used at high fields (11 kG$<B<$70 kG). It measures the magnetic moment directly as an induced voltage proportional to dM/dt.

[22] W. Shockley and W. T. Read, Phys. Rev. 87, 835 (1952).

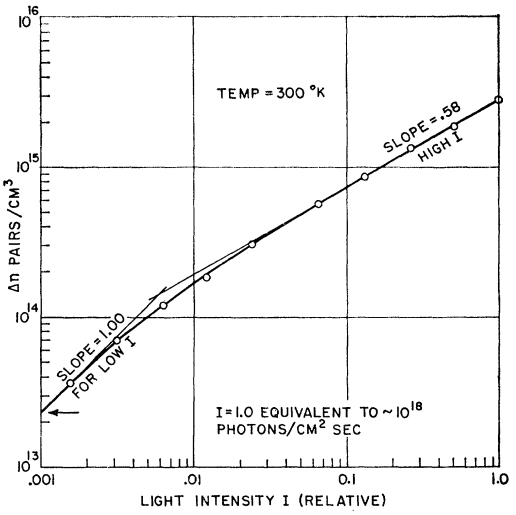

FIG. 5. Photopair density as a function of light intensity obtained by measurement of the photoconductivity.

tion range that $10^{14}<\Delta n<10^{15}$ cm^{-3}, the range over which Δn is approximately proportional to $I^{1/2}$.

The variation of Δn with temperature at constant (white) light intensity was also investigated for several crystals by means of the dc photoconductivity method. In order to avoid contact problems which are particularly bothersome at the lower temperatures, both voltage and current probes were used. These experiments were performed in the magnetic-moment equipment so that the light intensity was known to be the same as that used for the photomagnetism work. Temperature was measured with a thermocouple attached to the sample. Figure 6 shows Δn versus T at the maximum light intensity available. The reduction of Δn with decreasing temperature is due to the combined effect of falling bulk lifetime, rising surface recombination, and shift of the absorption band edge toward shorter wavelength as the temperature is lowered. Whatever the cause, these data are needed to compute the specific contribution per pair to the magnetic moment.

An equally important parameter is the surface recombination velocity, S, which is a measure of the rate at which pairs recombine on the surfaces of the sample.

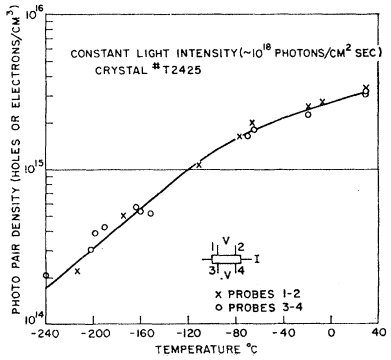

FIG. 6. Photopair density as a function of temperature at constant high light intensity. Dc photoconductivity method used.

The value of S strongly depends on surface conditions. While values for S are known in a general way for various etching treatments, the specific influence of S is so important to the understanding of the photomagnetism [Eq. (25)] that a separate study was undertaken to determine surface recombination velocity for the etch used and for the actual conditions of the experiment.

The surfaces of all the germanium samples used in the experiments were etched with RCA No. 5 etch.[23] This etch is applied immediately after a bright etch treatment with a HF, HNO_3-type etch which removes surface damage from grinding the crystals to size. This combination of bright etch and No. 5 was chosen because of the relatively low S attainable. It was found that S is strongly influenced by pair concentration at the surface.[24] Since the photomagnetism experiments were performed at high light levels, this variation of S has an important bearing on the interpretation of the results.

S was determined by the pulse photoconductivity method in which the total filament lifetime τ_f[18] is

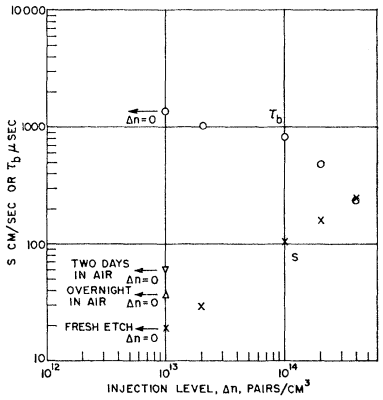

FIG. 7. Surface recombination velocity and bulk recombination lifetime versus injection level. The measurements were made in a helium atmosphere; aging after etching was in air. Data are for room temperature.

measured on several samples of the same material treated with the same etch, but having different dimensions. The variation of surface to volume ratio permits separate determination of τ and S. The method uses a short light pulse on the sample to yield a nonequilibrium change in carrier concentration which thereafter decays at the characteristic rate determined by τ_f. The conductivity, measured as a function of time, is used to find τ_f. The average injection level was set by illuminating the sample with steady light, simultaneously with the application of the light pulse. The magnitude of the injection was determined by the corresponding change in the dc conductance. The light pulse was of low intensity compared to the steady light.

Figure 7 shows the rapid increase of S as the injection level is raised. Immediately after etching, at zero injection level (in the dark), S is indeed very low ($S\sim 15$ to 20 cm/sec). As the injection level goes up, S rises at a

[23] S. G. Ellis, J. Appl. Phys. **28**, 1262 (1957).
[24] G. L. Dousmanis, J. Appl. Phys. **30**, 180 (1958).

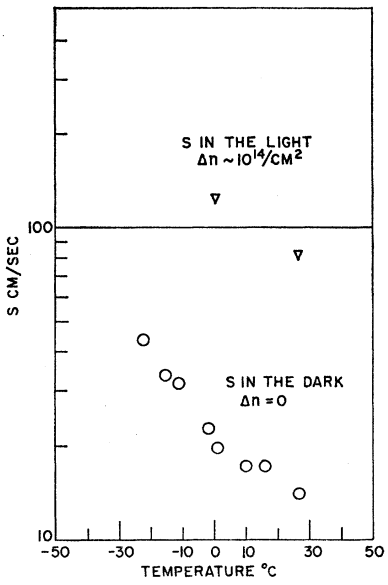

FIG. 8. Surface recombination velocity dependence on sample temperature. Measurements under high injection conditions, while not complete, indicate the same trend as for small injection.

slightly less than linear rate until, at the maximum level measured ($\Delta n = 4\times10^{14}/\text{cm}^3$), it has reached 250 cm/sec. Thus, the surface recombination velocity is not a unique constant of the material and surface treatment. Furthermore, there is some variation of S with aging, ambient atmosphere, and particularly with temperature. This variation causes some nonreproducibility in the absolute magnitudes of our measurements. As the temperature is lowered, S increases. This is shown in Fig. 8. Our measurements give results similar to those of Fan, Navon, and Bray.[25]

Figure 7 also shows τ as a function of injection. This result agrees with that obtained from dc photoconductivity, Fig. 5, in that $\tau \propto 1/\Delta n$ when $\Delta n \gg n_0$. τ is also a function of temperature,[25] in general decreasing exponentially as a function of $1/T$.

The mobilities and diffusion coefficients of holes and electrons are well known for relatively pure germanium.[26] In particular, $\mu_e \propto T^{-1.66}$ and $\mu_p \propto T^{-2.3}$, where $\mu_e \equiv |\mu_n|$, the absolute value of the electron mobility, and μ_p is the hole mobility. The factor $kT\mu_p\mu_e \propto T^{-3}$ determines the variation of the photomagnetic moment with T for $\mu_e\mu_p B^2 \ll 1$.

An important parameter in the theory is SL/D, where $L=(D\tau)^{1/2}$ is the diffusion length and D is the ambipolar diffusion coefficient. Our data combined with measurements in the literature, yield a reasonable estimate of the course of this quantity as a function of temperature. Figure 9 shows that SL/D is roughly constant and small from room temperature down to $\sim$150°K, then rises rapidly as temperature is lowered. $SL/D>1$ at $T<100$°K. This curve is not intended to apply in detail to all samples, since both S and τ are rather sensitive parameters. But the general trend of the composite SL/D is likely to hold for all fairly pure germanium samples etched in the fashion described. The photomagnetic moment is affected by the general shape of the SL/D curve, but does not depend too strongly on the absolute magnitude in the observed range (Fig. 2).

[25] H. Y. Fan, D. Navon, H. Gebbie, Physica **20**, 855 (1954).
[26] F. J. Morin, Phys. Rev. **93**, 62 (1954).

C. Results of Force Measurements

The force arising from the interaction of the photomagnetic moment M with the gradient of the magnetic field was measured explicitly as a function of the temperature, the magnetic field strength, and the light intensity (corresponding to carrier density). The observed dependence of M on these parameters, together with the values of the intrinsic germanium parameters discussed in the previous section, permit a detailed comparison with the theory. Most of the data are presented in relative terms, i.e., relative magnetic moment and relative light intensity. They can always be converted to absolute terms by remembering that a light level of 10^{18} photons/cm² sec ($\approx$0.1 W/cm²) giving rise to 10^{15} pairs/cm³, yields a photomagnetic moment $M \approx 5\times10^{-5}$ cgs/unit volume at a field of 10 kG, in the room temperature linear region. Absolute measurements of the force were not made with all specimens. Those that were measured absolutely gave considerable scatter of absolute magnitudes. This scatter was probably due to variations in S and τ. It is inferred that the absolute magnitude of the moment measured on several specimens apply to all specimens within at least a factor of 2. The relative quantities, which contain the dependence of M on T and B, are almost completely adequate to compare the experiment with the theory.

In these experiments, the sample was suspended in a helium exchange-gas atmosphere, while the walls of the chamber remained at room temperature or were cooled with liquid N_2 or liquid He. Because of the rather large heat input to the sample from the powerful light beam, the germanium never ran at the temperature of the ex-

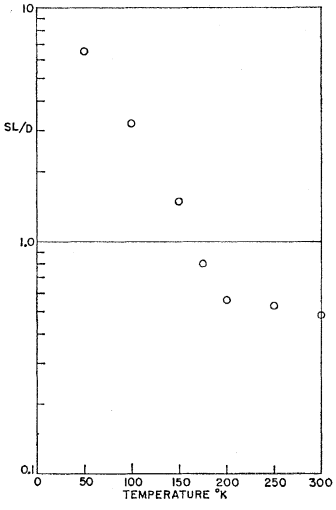

FIG. 9. SL/D, the important recombination parameter in the theory, as a function of temperature.

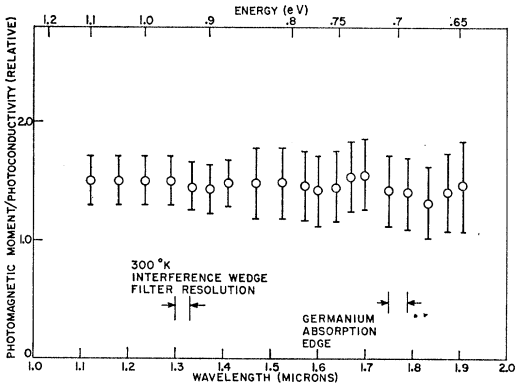

FIG. 10. Comparison of the photomagnetic moment with the photoconductivity. Dependence of the ratio on the spectral character of the exciting light.

change gas. A thermocouple was soldered to the sample and the fine wire leads were run up through the hollow glass suspension rod.[19] Thus, the force on the specimen in the field and its temperature could be recorded simultaneously, even while the sample was heated above ambient by the heat absorbed from the beam. Fluctuations in specimen temperature at the (16 cps) light input rate are very small, due to the high heat conductivity of germanium. For the same reason, the steady temperature gradient between the front and back of the specimen is also very small.

A large aperture wedge interference filter system was employed to measure the wavelength dependence of the ratio of photoconductivity to photomagnetic force (the light intensity available from a standard monochromator proved insufficient). The ratio measurement avoids the necessity for absolute calibration or correction of the lamp and optical system light intensities versus wavelength. The results plotted in Fig. 10 imply that, within experimental error, the photomagnetism is directly related to the carrier density, as expected from the theory.

An initially puzzling fact[4] was the observation that the photomagnetic moment was almost proportional to I (as shown in Fig. 11), while Δn from photoconductivity data was proportional to $I^{1/2}$ (see Fig. 5). The early conclusion was that this meant that $\Delta M \sim \Delta n^2$, implying an association of a free hole and a free electron ($\Delta n = \Delta p$). Later, more comprehensive data showed that the moment could vary as I^m with $0.7 < m < 1$, depending on the sample, while Δn varied as I^q, with $\frac{1}{2} < q < \frac{2}{3}$. These data were taken at room temperature where $(\mu_e \mu_p)^{1/2} B \ll 1$ even at 10 kG. Neutral screen filters were used to attenuate I.

If we consider only the intensity dependent terms in Eq. (25) under conditions where $(\mu_e \mu_p)^{1/2} B \ll 1$ (room temperature, $B \sim 10$ kG or less, for example) we find that $M \propto (S_R L/D)(1+S_R L/D)^{-1}(1+S_z L/D)^{-1} I\tau$. The factor $(1+S_z L/D)^{-1} I\tau$ is just equal to Δn, however, and if $S_R L/D \ll 1$ (of the order of a few tenths) and $S = S_R = S_z$, then $M \propto \Delta n(SL/D)$. Our independent data on S and τ versus I (see Fig. 7) show $SL/D \equiv S(\tau/D)^{1/2} \propto \Delta n(1/\Delta n)^{1/2} \propto \Delta n^{1/2}$ over the light intensity range of interest, i.e., 10^{14} to 10^{15} pairs/cm^3 generated. Hence $M \propto \Delta n^{3/2}$. If $\Delta n \propto I^{1/2}$, then $M \propto I^{3/4}$, while if $\Delta n \propto I^{2/3}$, $M \propto I$. In general, $\Delta n \propto I^q$ leads to $M \propto I^m$ with $m = \frac{3}{2}q$. In the example given in Figs. 5 and 11, $q = 0.58$, which leads one to expect $m = 0.87$. The observed value was $m = 0.9$. Thus, the observed power-law dependence of M on I is consistent with Eq. (25) and does not imply the presence of hole-electron complexes.

It is clear from the foregoing discussion that one cannot separately measure the variation of the photomagnetic moment with each of the parameters of the theory, since all except B vary with T, which itself is one of the fundamental parameters. The primary experimental data relating to the magnetic form factor of M were obtained in the form of curves of force versus magnetic field at constant generating light intensity, and with temperature as running parameter. In our presentation we plot equivalent magnetic moment $M = \text{Force} \times (\partial B_z/\partial y)^{-1}$. Typical primary data are shown in Fig. 12. It is evident that the departure from linearity which occurs as $\mu_e \mu_p B^2 \rightarrow 1$ becomes marked at high fields and low temperatures. At sufficiently small B, M/B is constant, as expected.

Figure 12 gives an erroneous impression about the comparative magnitudes of the magnetic moment at different temperatures. Although the light intensity was the same for all temperatures, the corresponding pair density generated by the light is itself a function of temperature, as already shown in Fig. 6. If we combine the magnetic-moment data with the pair-density data to give the magnetic moment per pair as a function of temperature, we show the temperature dependence in a more meaningful way. Figure 13 is a set of such curves with magnetic field as the parameter. At low fields, the data follow a T^{-3} dependence fairly accurately. As the field is raised, the influence of the magnetic saturation becomes evident at higher and higher temperatures, although the T^{-3} trend is still plain. Thus, we can say

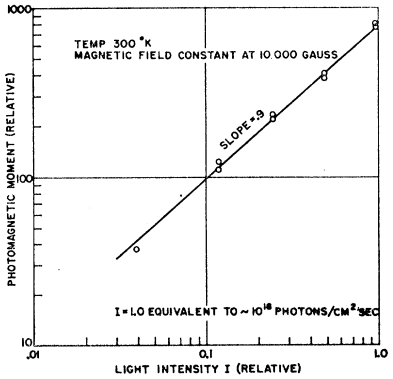

FIG. 11. Photomagnetic moment versus light intensity at constant temperature and magnetic field. A representative sample is shown. Slightly different slopes were obtained on other samples (see text).

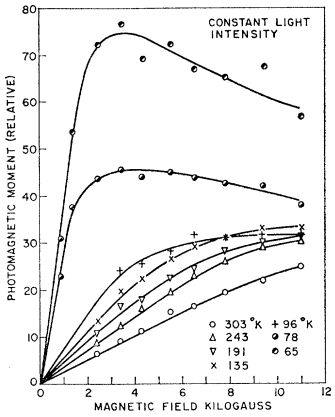

FIG. 12. The relative photomagnetic moment versus magnetic field for one sample at a series of temperatures.

that over that region in which the moment is proportional to field, the photomagnetic moment per unit pair is proportional to T^{-3}. This proportionality is exactly as expected from Eq. (25), from the fact that $kT\mu_p\mu_e \propto T^{-3}$, and that $(SL/D)(1+SL/D)^{-1}$ varies only slowly with T.

Ignoring the absolute magnitude of M, one may consider only the shape factor

$$(S_RL/D)(\mu_e\mu_p)^{1/2}B(1+\mu_e\mu_pB^2)^{-1/2} \times[1+(S_RL/D)(1+\mu_e\mu_pB^2)^{1/2}]^{-1}.$$

This quantity is plotted in Fig. 14, as a function of B, for selected values of T. The appropriate values of μ_p, μ_e, and S_RL/D have been inserted at each T value. Figure 14 is to be compared insofar as shape is concerned with Fig. 12 which plots the experimentally observed moment.

A somewhat more meaningful comparison with experiment can be made by plotting this shape factor as a function of $(\mu_e\mu_p)^{1/2}B$ rather than as a function of B alone (Fig. 15). By choosing a single value of SL/D most representative for the entire temperature range, the temperature parameter is suppressed and all of the calculated curves of Fig. 14 can be represented on a single curve. The set of experimental points for one crystal over the range 300 to 65°K shown in Fig. 12 has also been replotted. Relative magnitudes of the moment have been adjusted by a scale factor at each temperature so that the points fall on the calculated line at low fields (the linear range). Thus, this curve is again only a test of the shape factor and not of absolute or relative magnitudes. It is seen that again theory and experiment match rather closely, except when $\mu_p\mu_eB^2$ becomes appreciably greater than unity. It is thought that this departure may be due to a departure in that region of the magnetic moment from the formula [Eq. (25)], due to a direct effect of ∇B on M. The oversimplification of choosing a constant SL/D cannot account for the discrepancy. It is also possible that mobility anisotropy, ignored in the theory, is beginning to play an important part.

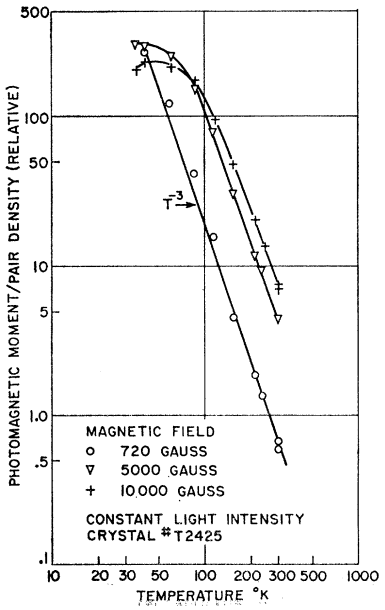

FIG. 13. The relative photomagnetic moment per unit generated pair as a function of temperature at constant light intensity. The solid line for the low-field case is a T^{-3} law.

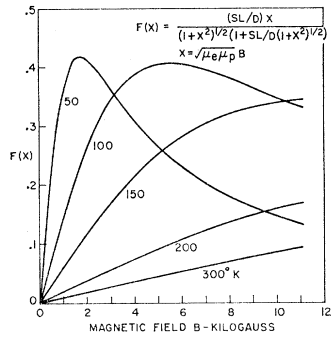

FIG. 14. The same function $F(x)$ as in Fig. 2 (Eq. 25) except plotted against the magnetic field with temperature as a parameter. The variation of SL/D, μ_e, and μ_p with temperature is included implicitly in the graph. Only the surface recombination velocity of the cylindrical edge is being considered here. The curve at each temperature is to be compared to the experimental data of Fig. 12 only as to shape. The magnitudes have not been corrected for the fact that the pair generation varies also with temperature (see Fig. 6).

D. Results of Direct Magnetic-Moment Measurements

Certain simplifications in the comparison of theory and experiment are possible in the direct induction measurements, since all were performed at room temperature. The variation of $\mu_p\mu_eB^2$ from less than to more than unity was achieved by varying the field strength only. As a result, SL/D, μ_p, and μ_e did not vary in the course of the experiment. It should also be noted that B was uniform in these experiments. For the case in which all surfaces of the sample were well etched (Fig. 16), no great error is made by taking $SL/D \cong 0$. Then the field-dependent factor in Eq. (25) simplifies to $\mu_e\mu_pB/(1+\mu_e\mu_pB^2)^{1/2}$ which saturates but does not go through

a maximum with increasing B. This factor is shown as the solid line on Fig. 16 along with the experimental points.

If S_z is maintained at a low value, but S_R is greatly increased (by sandblasting the lateral surfaces of the specimens), the amplitude or carrier density term in M [Eq. (25)] remains unchanged. The shape factor, however, becomes $(\mu_p\mu_e B)/(1+\mu_p\mu_e B^2)$, since $(S_R L/D)\rightarrow\infty$. The results of this experiment are plotted in Fig. 17, where the solid line represents the theory. It is seen that M goes through a maximum and the position of the maximum, $[(\mu_e\mu_p)^{1/2}B=1]$, is well predicted by the theory.

Another test of the applicability of Eq. (25) can be made by considering the ratio of the signal magnitude for the two cases of low and high S_R, i.e., etched/sandblasted edge for the same sample at constant temperature, light level and small but constant field $[(\mu_e\mu_p)^{1/2}B\ll 1]$. This ratio should be

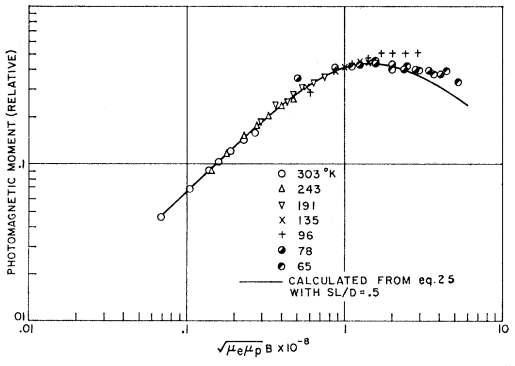

FIG. 15. Photomagnetic moment versus $(\mu_e\mu_p)^{1/2}B$. At each temperature the set of points have been normalized to fall on the linear curve for small $(\mu_e\mu_p)^{1/2}B$. Note that at high $(\mu_e\mu_p)^{1/2}B$, the calculated curve falls off more rapidly than the experimental data.

$$\frac{S_R L/D}{1+S_R L/D}:1.$$

The observed ratio was $\frac{1}{4}$, which implies $S_R L/D\approx 0.33$ for the etched case. The independently measured value of SL/D by pulse photoconductivity on a similar sample was 0.48 (see Fig. 9). We consider this reasonable self-consistency.

Finally, we can compute the absolute magnitude of the photodiamagnetism at room temperature using the self-consistent estimate of SL/D and the photoconductivity value of Δn. Use of the latter eliminates the necessity of determining the absolute light intensity. For a field of 10 kG and pair density of $10^{15}/\text{cm}^3$, $M=9.0\times10^{-5}$ G/cm^3 corresponding to a susceptibility change of 9.0×10^{-9} cgs units per unit volume which is in reasonable agreement with both the static- and pulse-magnetic data.

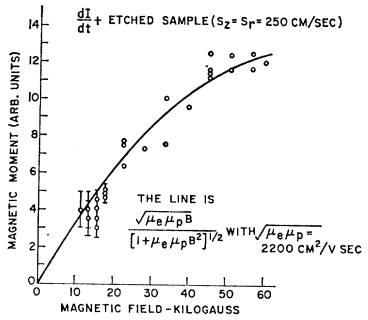

FIG. 16. Photomagnetic moment obtained by the induction method versus magnetic field. For this curve, all surfaces of the sample were well-etched. Data were taken at room temperature.

CONCLUSIONS

The magnetic moment of a plasma in steady-state transport transverse to and along a magnetic field was derived by means of the macroscopic drift equations, and the particle conservation and boundary conditions appropriate for semiconductor crystals. In this derivation, we assumed a constant scattering time, explicitly introduced through the generally accepted conductivity mobilities. Two types of experiments were used to compare this theoretical magnetic moment with the actual moment of a hole-electron plasma infected by light into germanium crystals. The agreement found was as good as could be expected from the accuracy of the experiments. The agreement of theoretical and experimental shape factors was generally excellent. Agreement in absolute magnitude was more difficult to establish, due to drifts in the semiconductor surface recombination velocity—resulting in drifts in the absolute carrier density. There is, however, no implication in the data that the theoretical and experimental amplitudes of M show any discrepancy.

The major area of disagreement occurred in measurements of M, using the inhomogeneous field—force method at large values of $(\omega_i\tau_i)^2\equiv\mu_e\mu_p B^2=\omega_e\tau_e\omega_p\tau_p$, where ω_i is the cyclotron frequency and τ_i the scattering time (Fig. 15). It is likely that the discrepancy observed

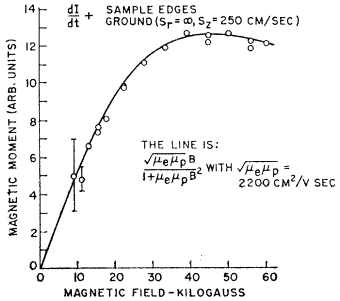

FIG. 17. Photomagnetic moment obtained by the induction method versus magnetic field. The sample is the same as for Fig. 16, but the cylindrical edges were sandblasted to make $S_R=\infty$, while the ends of the cylinder remained well-etched ($S_z=250$ cm/sec). Note the distinct maximum in the curve.

is due to the effect of the curvature of B, which was neglected in the derivation of M. It can be shown that this curvature effect is negligible at small $\omega_i\tau_i$. However, when $\omega_i\tau_i \to \infty$, the curvature of the field together with the gradient yields twice the effective transverse particle drift velocity obtained with ∇B_z alone.[27] The transverse drift, in the microscopic description of the plasma, generates the net force in an inhomogeneous field. One would, thus, expect the effective M, derived from the force, not to fall as rapidly with increasing $\omega_i\tau_i$ as expected from the simple theory. This view is supported by the observation that the M measured by the induction method in a uniform field B was not at variance with the theory (Fig. 17).

It is also possible that the simple approach adopted here of uniting the flow equations in the magnetic field is not correct since it essentially ignores the scattering mechanism which contributes to the mobility variation with temperature. Kurnick and Zitter[15] investigated this for the semiconductor InSb by proceeding through the current-density equations of transverse magnetoresistance and Hall effect putting in a relaxation time proportional to v^{-1} (thermal scattering) and to v^3 (impurity scattering). However, in both cases, the result calculated for the PEM effect, which is closely related to the photomagnetism, was in poorer agreement with experiment than the simple theory. It is probable, therefore, that this approach would not remove the discrepancy.

It is evident from the general agreement of theory and experiment that the over-all description of the physical phenomena is correct. Regarded from the plasma point of view, this constitutes the first experiment which directly measures the diamagnetic force exerted by the plasma on its scattering medium, if the magnetic field is inhomogenous. Apart from the field curvature effect this force is identical to the expanding force of a fully ionized gas (no appreciable neutral scattering).[9]

In the semiconductor case, the variation of the surface recombination velocity, which may also be considered a reflection coefficient, furthermore clearly demonstrates the transition between steady state and thermal equilibrium conditions. When $S \to \infty$ in Eq. (25), the usual "plasma" state is reached; $S \to 0$ is the thermal equilibrium limit. The "wall contributions" to the magnetic moment are therefore explicitly apparent in our case. In the gas plasma this clear distinction cannot readily be made.

From the semiconductor point of view, it is clear that unless the condition $SL/D \to 0$ can be achieved, it is not possible to measure equilibrium magnetic properties of carriers by the present method. Since the Landau magnetic moment is overshadowed by the nonequilibrium effects, it is clearly necessary to measure it by the equilibrium methods already tried. Our explanation of early observations in terms of an anomalous equilibrium effect[5] was based on the unwarranted supposition that $S \to 0$. The "size effect,"[5] which was interpreted in terms the anomalous equilibrium effects, is also simply explained in terms of the complete steady state diffusion theory (see Appendix II).

[27] See Ref. 16, p. 55.

ACKNOWLEDGMENTS

We would like to acknowledge helpful discussions with R. Parmenter, M. Lampert, D. O. North, and S. Yoshikawa. B. E. Tompkins provided invaluable assistance in design, construction, and operation of the experimental equipment. W. Merz of Laboratories RCA, Zurich was also helpful in the pulsed magnetic-field work. F. Herzfeld originated the computer program for the calculation in Appendix II.

APPENDIX I: INDUCTION METHOD FOR MEASURING M

Consider a germanium specimen surrounded by a pick-up coil of N turns, immersed in a time-varying field $\mathbf{H}(t)$, and illuminated by a light beam of time-varying intensity $I(t)$ (Fig. 4). The light, as before, serves to inject a plasma of holes and electrons. The EMF induced in the coil is $V=-10^{-8}\times NAdB/dt$ V. It is assumed that the whole coil area A (in cm^2) is filled with germanium. Since $B=H+4\pi M$,

$$V=-10^{-8}NA[dH/dt+4\pi dM/dt]. \tag{27}$$

The experimental arrangement is designed to measure $M(t)$ via the second term in this expression. The variation of M with time is given by $dM/dt=(dM/dI)\times(dI/dt)$. The first term in Eq. (27) is balanced by a second pick-up coil, not containing a specimen, and located symmetrically in the field relative to the first. The dH/dt signals in the first and second coils can be made to cancel in an inductance bridge (Fig. 4). For perfect balance, the signal voltage is just

$$V=-4\pi\cdot 10^{-8}NA\,(dM/dI)dI/dt \text{ V}. \tag{28}$$

The quantity dI/dt can be measured separately by means of photoconductivity experiments on a piece of germanium similar to the moment specimen, located at the position of the magnetic test sample. In any case, it is not a function of magnetic field; so for purely relative measurements at constant light intensity, the measured voltage gives ΔM versus H directly.

One problem which must be considered is the effect of eddy currents in the sample due to dH/dt. Such eddy currents can have the same time dependence as Eq. (28) because of the modulation of the germanium conductivity by the light. The resultant apparent change in magnetic moment will also be picked up by the coil. It is easily shown that the expected voltage is

$$V_{\text{eddy}} \propto \frac{d}{dt}\left(\sigma\frac{dH}{dt}\right)=\frac{d\sigma}{dt}\frac{dH}{dt}+\sigma\frac{d^2H}{dt^2}, \tag{29}$$

where σ is the germanium conductivity. The first term can be of the same order as V in Eq. (28), while the second term is at least 50 times smaller. In the experiment, the time delay circuit in Fig. 2 was therefore adjusted so that the light flashed exactly when $dH/dt=0$, i.e., at the peak of the magnetic-field discharge. This removed the eddy current contribution.

A practical problem encountered was the difficulty of exactly balancing out the first term in Eq. (27) inasmuch as it can be 10^4 times larger than the second term. After balancing the bridge as carefully as possible, the residual was still ten times larger than the signal sought. However, the first term has the period of the field variation, which is about ten times longer than the major frequency components of the moment variation. Hence, careful restriction of the low-frequency response of the amplifier reduced the level of the dH/dt term in Eq. (27) without affecting the dM/dt term, yielding the required signal on an almost flat base line. At the highest fields some base line variation was nevertheless observable. The upper frequency cutoff was also restricted to reduce coil noise.

The inductance bridge voltage was measured with differential input on a type E plug-in unit for a Tektronix Type 532 oscilloscope. The pick-up coils used in the experiment were 1 cm^2 in cross section. Each was wound with 1400 turns of 0.07-mm wire. The light flash was of short duration compared with the free pair lifetime. The instant of flashing relative to the beginning of the field pulse was controlled by the time delay circuit and the gate delay of the scope. The field H was obtained by discharging 800 μf through coils 5-cm long, with 3-cm o.d. and 1.5-cm i.d. The specimens were cylindrical, 5 mm in radius and 1-cm long.

APPENDIX II: DERIVATION OF THE MAGNETIC MOMENT APPLICABLE TO CYLINDERS OF ANY HEIGHT (RESTRICTION $\zeta\rightarrow\infty$ REMOVED)

The correct particle conservation equation with z dependence included is simply $\nabla\cdot n\mathbf{v}=-n/\tau$, where $\mathbf{v}$ is the macroscopic drift velocity of the positive particles, derived under the ambipolar flow conditions, τ is the recombination lifetime, and $n=n(r,z)$. This replaces Eqs. (17) and (20) in which the z and r dependence was separated. The incident light produces I pairs/cm^2/sec uniformly across the front face of the cylinder of Fig. 1, in a thickness $\ll L\equiv(D\tau)^{1/2}$. We assume steady-state conditions. In cylindrical geometry,

$$-\left[\frac{1}{r}\frac{\partial}{\partial r}\left(r\frac{D}{1+\mu^2B^2}\frac{\partial n}{\partial r}\right)+\frac{\partial}{\partial z}D\frac{\partial n}{\partial z}\right]=-\frac{n}{\tau}. \tag{30}$$

Setting $\rho\equiv r(1+\mu^2B^2)^{1/2}\equiv r\beta^{1/2}$ and $n(r,z)=\lambda(\rho)\omega(z)$, Eq. (30) separates into

$$\frac{d^2\lambda}{d\rho^2}+\frac{1}{\rho}\frac{d\lambda}{d\rho}+\frac{\lambda}{\nu_m^2}=0 \tag{31}$$

and

$$\frac{d^2\omega}{dz^2}-\left(\frac{1}{L^2}+\frac{1}{\nu_m^2}\right)\omega=0, \tag{32}$$

where ν_m^{-2} is the separation constant. The boundary conditions are:

$$\begin{aligned}
&\text{(I)}\quad n(\rho,z)\text{ is finite within the cylinder;}\\
&\text{(II)}\quad -\frac{D}{\beta}\left[\frac{1}{n}\frac{\partial n}{\partial r}\right]_{r=R}=-\frac{D}{\beta^{1/2}}\left[\frac{1}{\lambda}\frac{d\lambda}{d\rho}\right]_{\rho=\beta^{1/2}R}=S_R;\\
&\text{(III)}\quad -\frac{D}{n}\frac{\partial n}{\partial z}\Big]_{z=0}=\frac{I}{n}\Big]_{z=0}-S_z;\\
&\text{(IV)}\quad -\frac{D}{n}\frac{\partial n}{\partial z}\Big]_{z=\zeta}=S_z.
\end{aligned} \tag{33}$$

Using condition (I), and setting $\nu_m^{-2}+L^{-2}=K_m^{-2}$, we find

$$\begin{aligned}
&\lambda(\rho)=J_0(\rho/\nu_m),\\
&\omega(z)=A_m\cosh(z/K_m)+B_m\sinh(z/K_m),
\end{aligned} \tag{34}$$

where the ν_m, A_m, and B_m are constants to be determined. Condition (II) determines the ν_m:

$$\frac{Q}{\nu_m}\frac{J_1(Q/\nu_m)}{J_0(Q/\nu_m)}=\frac{S_RQ}{D}\beta^{1/2}, \tag{35}$$

where $Q\equiv R\beta^{1/2}$. Boundary conditions (III) and (IV) must be satisfied simultaneously. This requires expansion of I in terms of the $J_0(\rho/\nu_m)$. We use Eq. (35) and the orthonormality conditions to obtain

$$\int_0^R rdr\,J_0(r\beta^{1/2}/\nu_m)=(\nu_mR/\beta^{1/2})J_1(Q/\nu_m)$$

and

$$\int_0^R J_0(r\beta^{1/2}/\nu_m)J_0(r\beta^{1/2}/\nu_n)rdr=\delta_{mn}(R^2/2)[J_1^2(Q/\nu_m)+J_0^2(Q/\nu_m)].$$

Then with $a_m\equiv(S_zK_m/D)$ and

$$\gamma_m=\frac{2\nu_mI}{Q}\frac{J_1(Q/\nu_m)}{J_0^2(Q/\nu_m)+J_1^2(Q/\nu_m)},$$

(III) and (IV) become

$$\begin{aligned}
&a_mA_m-B_m=(\gamma_mK_m/D),\\
&A_m[\sinh(\zeta/K_m)+a_m\cosh(\zeta/K_m)]\\
&\quad+B_m[\cosh(\zeta/K_m)+a_m\sinh(\zeta/K_m)]=0.
\end{aligned} \tag{36}$$

Equation (36) determines the A_m and B_m which, to-

gether with Eq. (34), yields $n(r,z)$:

$$n(r,z)=\sum_{m=0}^{\infty} J_0\left(\frac{r\beta^{1/2}}{\nu_m}\right)\left[\frac{2\nu_m I}{Q}\frac{K_m}{D}\frac{J_1(Q/\nu_m)}{J_0^2(Q/\nu_m)+J_1^2(Q/\nu_m)}\right]f_m(z),$$
$$f_m(z)=\frac{\cosh(z/K_m)[\cosh(\zeta/K_m)+a_m\sinh(\zeta/K_m)]-\sinh(z/K_m)[\sinh(\zeta/K_m)+a_m\cosh(\zeta/K_m)]}{2a_m\cosh(\zeta/K_m)+(1+a_m^2)\sinh(\zeta/K_m)}. \tag{37}$$

To compute the magnetic moment we require the integral

$$g(R,\zeta)=\int_0^{\zeta} dz\int_0^{R} r^2\frac{\partial n}{\partial r}dr;$$

[see Eq. (13)]. Using Eq. (37) we obtain

$$g(R,\zeta)=\sum_{m=0}^{\infty}\frac{2I}{D}\frac{S_R R}{D}\nu_m^2 K_m^2\left[\frac{1-2\left(\frac{\nu_m}{R}\right)^2\left(\frac{S_R R}{D}\right)}{1+\left(\frac{\nu_m}{R}\right)^2\times\left(\frac{S_R R}{D}\right)^2(1+\mu^2B^2)}\right]\left[\frac{a_m\cosh(\zeta/K_m)+\sinh(\zeta/K_m)-a_m}{2a_m\cosh(\zeta/K_m)+(1+a_m^2)\sinh(\zeta/K_m)}\right]. \tag{38}$$

The magnetic moment **M** is then obtained from Eq. (13) as

$$\mathbf{M}=\hat{\mathbf{Z}}\frac{e(\mu_p+|\mu_n|)DB}{R^2\zeta}g(R,\zeta). \tag{39}$$

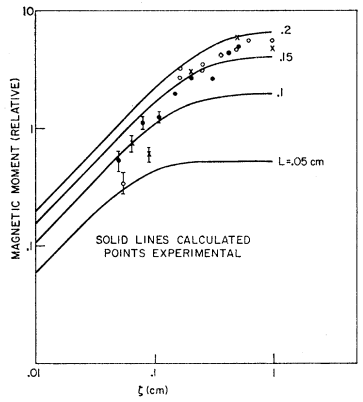

FIG. 18. Comparison of calculated and measured magnetic moment as functions of sample thickness. Solid lines machine-computed from Eqs. (38) and (39). Parameters: $SL/D=0.5$, $R=0.5$, $\mu B\ll 1(\beta=1)$. Experimental points from three runs. Room temperature, $SL/D=0.5$, $L=0.15$, $R=0.5$ (independently determined). Theoretical and experimental curves matched at one point for best fit.

The sum in Eq. (38) contains the dependence of the magnetic moment on sample dimensions and surface recombination and is, therefore, subject to experimental test. In fact, the moment had already been measured in Ref. 5 as a function of sample thickness ζ, although given a different interpretation. This experiment was repeated and the new experimental points together with the original ones are shown in Fig. 18. An important change in the value of the diffusion length has been made. The diffusion length was given in Ref. 5 as 0.06 cm, but this was in error due to the incorrect estimate of the surface recombination velocity. When the correct value is used, as given in Fig. 7 for high injected densities, the corrected value of L is 0.15 cm. The sum was computed on the IBM 7090 using the measured values of the parameters: $S_R=S_z=S$, $SL/D=0.5$, $R=0.5$ cm, $\mu B\ll 1$. The solid lines in Fig. 18 show the result for the relative magnetic moment for various choices of L. The moment falls off as sample thickness is decreased, as observed experimentally. The experimental values apparently fall off a little more rapidly than the choice of $L=0.15$ cm would predict, although the general trend is reproduced fairly well. Thus, we believe that this "size effect" is also explicable by the general theory given in this paper.